

RESEARCH

Open Access



# An Anchorage Technique for Shear Strengthening of RC T-Beams Using NSM-BFRP Bars and BFRP Sheet

Hesham M. Diab<sup>1\*</sup> and Ahmed M. Sayed<sup>1,2</sup>

## Abstract

This study presents a detailed experimental program for reinforced concrete T-beams strengthened in shear with near-surface mounted (NSM) basalt fiber-reinforced polymer (BFRP) bars. This paper aims to introduce and evaluate a nonmechanical anchorage technique for shear strengthening using NSM-BFRP bars. T-beams were strengthened using manually manufactured closed or U-shaped hybrid BFRP stirrups (BFRP bars and BFRP sheets). The experimental program was developed to study the effects of these anchorage techniques. The results showed that the shear capacity increased by 8%–46% for beams strengthened with NSM-BFRP bars without anchorage. However, the presence of the proposed anchorage system increased the shear capacity of the strengthened beams by 39.6%–81.6%. Moreover, the maximum strains induced in the BFRP bars ranged from 27 to 59% of their ultimate strains according to the spacing between the NSM and the presence of the anchorage. The proposed anchorage technique prevented the premature debonding of the NSM-BFRP bars.

## 1 Introduction

Fiber-reinforced polymer (FRP) systems have been used worldwide for almost the last three decades and are becoming a widely accepted method for strengthening concrete structure in shear and flexure (Diab et al. 2009; Bilotta et al. 2015; Chen et al. 2018). Various experimental studies have been performed to examine the shear strengthening of concrete members using external bonding (EB) FRP sheets/strips (Kalfat et al. 2013; Shekarchi et al. 2018). However, the use of EB-FRP sheets/strips for strengthening concrete members is not entirely problem-free.

The use of near-surface mounted (NSM) fiber-reinforced polymer (FRP) bars is an attractive method for increasing the shear strength of shear-deficient reinforced concrete members. Shear strengthening of

reinforced concrete (RC) beams using NSM-FRP bars is more efficient than using externally bonding FRP sheets/plates (Rizzo and De Lorenzis 2009; Dias and Barros 2011). NSM-FRP bars/strips are less susceptible to damage from fire or vandalism, as they are embedded in the concrete cover. There are several types of FRP bars in the market, such as carbon (CFRP), glass (GFRP), aramid (AFRP), and basalt (BFRP) bars. Various experimental data are reported in terms of the enhancement in the shear load-carrying capacity for the strengthening of concrete beams using CFRP and GFRP with the NSM technique (Anwarul 2009; Sundararaja and Rajamohan 2009). However, the use of conventional CFRP and GFRP composite materials is hindered due to the high cost of CFRP and the poor creep and fatigue performance of GFRPs (Sim et al. 2005; Diab and Wu 2009; Elmahdy and Verleysen 2020). The creep rupture stress of GFRP is limited to 0.2 times its tensile stress according to ACI 440.1R-15 (2015). Although Wu et al. (2010) compared the fatigue behavior of various FRP composite sheets and found that the fatigue behavior of BFRP was comparable to that of conventional

\*Correspondence: heshamdiab2@yahoo.com

<sup>1</sup> Civil Engineering Department, Faculty of Engineering, Assiut University, Assiut, Egypt

Full list of author information is available at the end of the article

Journal information: ISSN 1976-0485 / eISSN 2234-1315

GFRP, Wang et al. (2014) investigated the creep behavior of BFRP for prestressing applications and concluded that the creep rupture stress of BFRP was 0.54 times its tensile strength. Recently, basalt fiber-reinforced polymer (BFRP) composites have become commercially available at a low cost and may represent an alternative to GFRP (Wang et al. 2017; Elmahdy and Verleysen 2020; Lebedev et al. 2020). Nevertheless, the experimental databases available in the literature for NSM of BFRP bars are very limited, and the current study presents a contribution to this database.

Three different failure modes were observed for beams strengthened in shear with NSM-FRP bars. The first failure mode was due to debonding between NSM bars and the epoxy associated with shear failure (De Lorenzis and Nanni 2001; Bianco et al. 2009; Rahal and Rumaih 2011) due to the low amount of FRP. However, the second failure mode, due to increasing the amount of FRP, was a separation of the parts of the concrete cover along with the NSM-FRP bar associated with shear failure (Barros and Dias 2006). The third failure mode was the delamination of the concrete cover, where the premature detachment of the concrete layer includes the FRP bars (De Lorenzis and Nanni 2001; Barros and Dias 2006; Dias and Barros 2011; Wiwatrojjanagul et al. 2012), which indicates that the efficiency of NSM-strengthened beams is restricted to the concrete strength and limited spacing between the NSM bars. All these types of shear failure modes can be prevented by using proper anchorage.

To date, most studies involving FRP anchors have been carried out for beams strengthened in shear with EB-FRP sheets/plates (Kalfat et al. 2013; Koutas and Triantafillou 2013; Shekarchi et al. 2018), and few studies have been carried out on the anchoring of NSM-FRP bars. Recently, shear strengthening of RC beams using NSM manually made FRP rods has been investigated by other researchers (Jalali et al. 2012; Sharbatdar and Jaber 2018). They focused on a newly developed anchorage “T-shaped anchor” for rectangular RC cross sections. They concluded that the use of the end anchors for NSM-FRP strengthening increased the contribution of the FRP on the shear capacity by approximately 60% compared with that of unanchored FRP bars. However, the failure modes were similar to those in previous studies. Although closed stirrups and U-shaped FRP bars around the beam cross section are the most effective strengthening solutions for NSM shear strengthening, they are rarely available with the required dimensions in practice. In Egypt, all the products of FRP bars are imported from outside of the country, and it is difficult to import the deformed bars,

which depend on the dimensions of each cross section of the shear-deficient beams.

## 2 Research Significance

This paper evaluates applying BFRP bars for the shear strengthening of RC T-beams using the NSM technique. Additionally, this paper introduces a manual anchor type for the strengthened beams with NSM-FRP bars. This anchor is made in the laboratory using BFRP bars and BFRP sheets to form closed stirrups or U-shaped stirrups. The effectiveness of NSM shear strengthening using hybrid BFRP stirrups is examined through an experimental study.

## 3 Experimental Program

### 3.1 Details of the Tested Beams

The shear failure of reinforced concrete beams strengthened with NSM-FRP bars is dependent on different variables. This study is limited to concerns regarding some of the most significant factors: (1) basalt FRP bars as a suitable shear strengthening material; (2) anchoring of NSM-FRP bars around the web and through the flange using a new anchorage technique; and (3) the spacing between NSM-BFRP bars. The main experimental program is composed of six shear-deficient RC T-beams. The different T-beams that are tested have the same dimensions and the same amount of internal reinforcement as well as typical arrangements. The T-cross section geometry, details of the steel reinforcement, longitudinal geometry, and longitudinal reinforcement of the tested beams are shown in Fig. 1. All the beams are 1450 mm long (1250 mm, effective span) and 300 mm in height (270 mm, the effective depth). The flange is 450 mm wide and 70 mm thick. The shear span  $a=430$  mm is constant for all the tested beams, and the shear span to depth ratio  $a/d$  is 1.6 to ensure shear failure.

The tested beams were reinforced in tension with five deformed steel bars that were 16 mm in diameter, three of which were bent 90° at both ends to achieve the anchorage criteria. Shear reinforcement was adopted to assure the shear failure mode for all the tested beams at the right side span (Fig. 1), where steel stirrups with a diameter of 6 mm and a spacing of 150 mm ( $\text{Ø}6@150$  mm) were applied. To avoid shear failure at the left side span (Fig. 1), steel stirrups with a diameter of 8 mm were applied on the left side with a spacing of 100 mm ( $\text{Ø}8@100$  mm). A three-point bending test setup for different shear span lengths was adopted to induce shear failure in one span (the right side). The following subsequent sections give the details for the

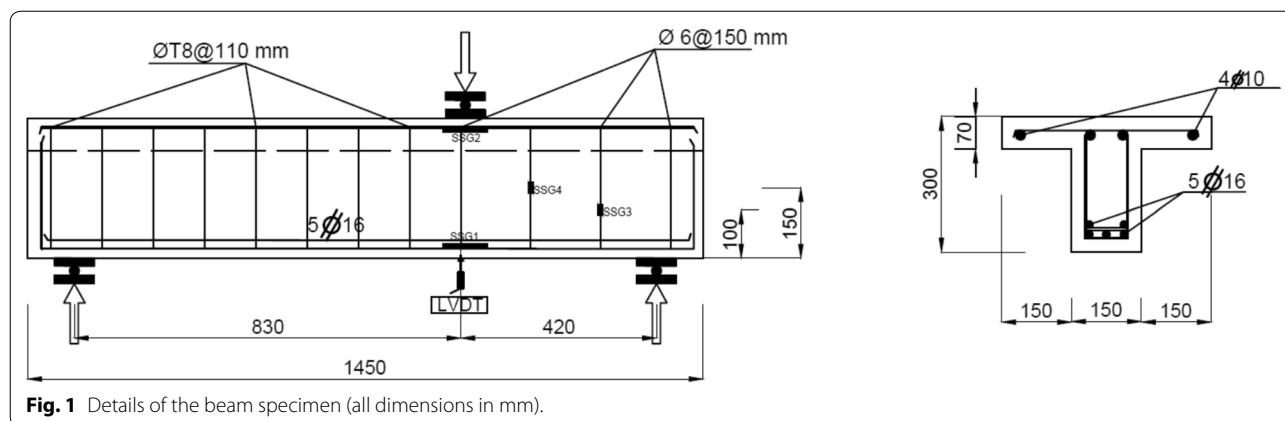


**Fig. 1** Details of the beam specimen (all dimensions in mm).

tested beams, their instrumentation, and the testing procedure in addition to the material properties.

### 3.2 Materials Properties

#### 3.2.1 Properties of the Concrete

The beams were made of concrete with a target compressive strength of 25 MPa. The 28-day compressive strength ( $F_{cu}$ ) and compressive strength on the day of testing the beams were calculated from the average values of three standard cubes with dimensions of 150 × 150 × 150 mm.

#### 3.2.2 Properties of the Steel Reinforcement

Table 1 presents the properties of the transverse and longitudinal steel reinforcement used in all the specimens. These values are the average of the three values obtained from the tension test according to ASTM A370-97a (1997) and Egyptian code (2007).

#### 3.2.3 Properties of the FRP Strengthening Materials

Two types of BFRP composites were used in this study. The first type was GBF® BFRP bars with 14 mm deformed bars (Fig. 2a), and the second type was BFRP sheets (BUF-300) produced in China (Shanxi Basalt Fiber Technology Co., Ltd.). The properties of the BFRP bars were experimentally determined according to the ACI 440.3R-04 guidelines (American Concrete Institute 2004). The total length of all the test specimens was 1000 mm, which included the free length (600 mm)

plus the two anchor lengths (200 mm for each). The steel tubes with diameters of 37.5 mm were filled with adhesive mortar (Kemapoxy 165. 2016), as shown in Fig. 2b. Three test specimens were made to evaluate the mechanical properties of the BFRP deformed bars. Three strain gauges and one clip gauge were mounted on the test section to measure the strains and displacement, respectively (Fig. 2b). The load, strain, and displacement were recorded by an electronic data acquisition system, as shown in Fig. 2c. All the specimens failed due to rupture of the BFRP bars, as shown in Fig. 2d. Based on the average of three test results, the tensile strength and modulus of elasticity of the BFRP bar (14 mm in diameter) are equal to 772 MPa and 59.7 GPa, with coefficients of variation (CV %) equal to 4.3% and 7.6%, respectively. These values yield an ultimate tensile strain of 1.29%. Table 2 summarizes the mechanical properties of the BFRP bars. The relationship between the tensile stress and the strains mounted on the BFRP bar is shown in Fig. 3. The strain results obtained from the clip gauge device gave accurate results compared with the results for the strains (1 and 3), which were affected by the rupture of the fibers. The test results showed that the stress–strain relationship of the BFRP bars was almost linear up to failure.

The other type was BFRP sheets (BUF-300), which were used to form closed stirrups or U-shaped stirrups with BFRP bars. The mechanical properties of the

**Table 1** Mechanical properties of the steel reinforcement.

Diameter (mm)	Type of steel	$f_y$ (MPa)	$f_u$ (MPa)	E (GPa)	Usage
Ø 6	Mild	360	522	204	Stirrups
Ø 8	Mild	326	485	200	Stirrups
Φ 10	High tensile	509	665	196	Compression steel
Φ 16	High tensile	542	638	203	Tension steel

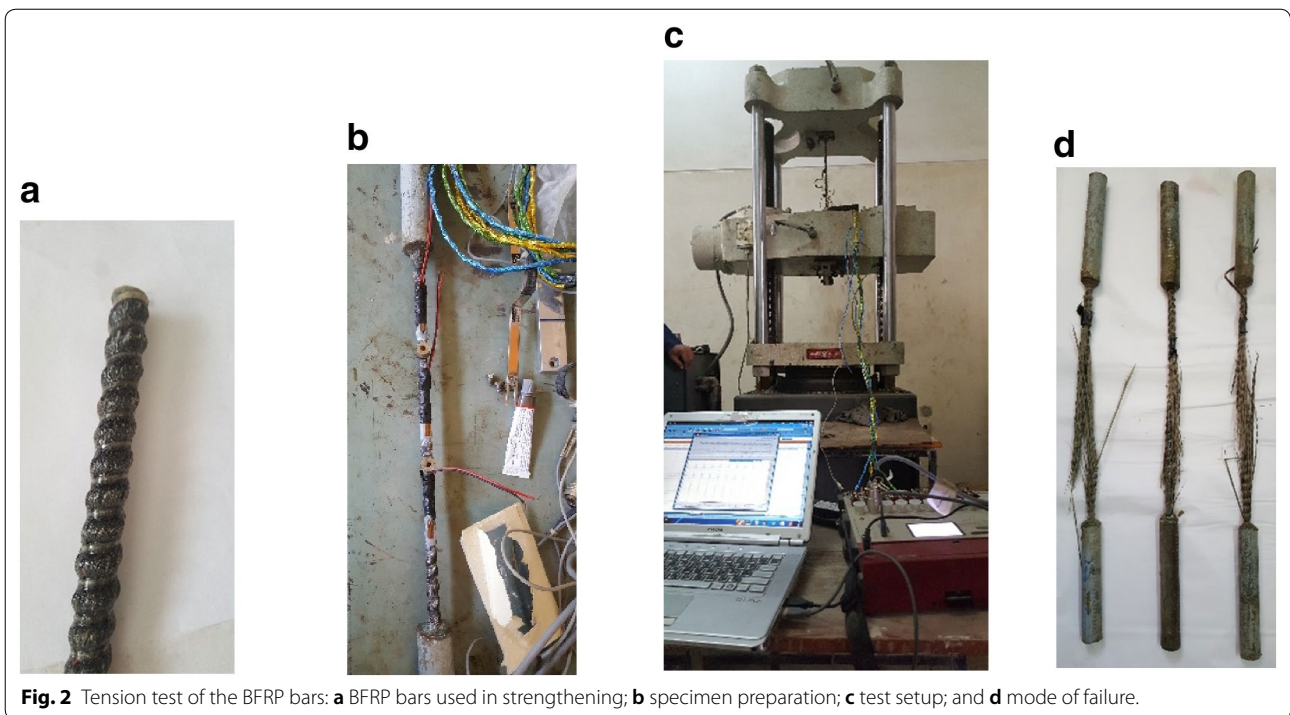


**Fig. 2** Tension test of the BFRP bars: **a** BFRP bars used in strengthening; **b** specimen preparation; **c** test setup; and **d** mode of failure.

**Table 2** Mechanical properties of the BFRP bars.

Type	Diameter (mm)	Modulus of elasticity (GPa)	Tensile strength (MPa)	Rupture strain (%)
BFRP-14	14	59.7	772	1.29

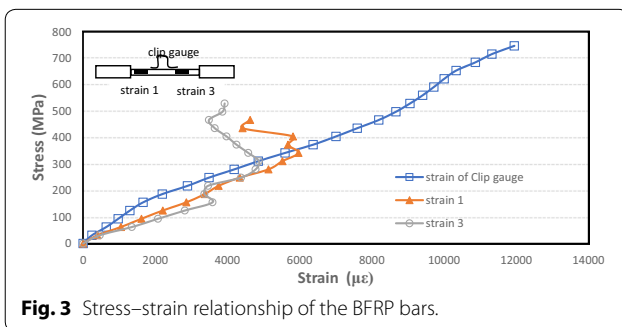


**Fig. 3** Stress-strain relationship of the BFRP bars.

**Table 3** Mechanical properties of the BFRP sheet.

Types of fibers	Fiber aerial weight (g/m <sup>2</sup> )	Thickness (mm)	Modulus of elasticity (GPa)	Tensile strength (MPa)	Rupture strain (%)
Basalt (BUF7-300)	300	0.17	91.0	2100	2.6

BFRP fibers and their nominal thickness are presented in Table 3. The properties of the fibers were provided by the manufacturer.

### 3.2.4 Properties of the Epoxy

A two-part epoxy (Sikadur<sup>®</sup> 30) was used as the adhesive filler to fix the BFRP bars inside the grooves. Furthermore, a two-part adhesive (Sikadur<sup>®</sup> 330) was used to wrap the BFRP sheet around the BFRP bars to form closed or U-shaped stirrups. Table 4 presents the properties of the epoxies provided by the manufacturer (Sikadur<sup>®</sup>-30; Sikadur<sup>®</sup>-330).

### 3.3 External Strengthening with NSM deformed BFRP stirrups

All different beams were strengthened using 14-mm deformed GBF<sup>®</sup> BFRP bars embedded in epoxy-filled grooves. Figure 4a shows the typical deformation of these bars. The spacing between the NSM reinforcement bars controls the failure mode of the NSM reinforcement (Dias and Barros 2010); therefore, two different spacings between the BFRP bars were examined, which were equal to 100 mm and 200 mm. To prevent debonding and increase the shear strength of the NSM-strengthened beams, anchorage for the NSM-BFRP bars was applied in this study. Three types of anchoring techniques were adopted in this study. (1) The BFRP bars were anchored using the embedded-through-section (ETS) method

**Table 4 Properties of the epoxy.**

Epoxy type	Mechanical properties	Values
Epoxy (sikadur® 30 [33])	Ultimate strength (MPa)	24–27 (15 °C); 26–31 (35 °C)
	Shear strength (MPa)	14–17 (15 °C); 16–19 (35 °C)
	Elastic modulus (GPa)	11.2 (23 °C)
Epoxy (sikadur® 330 [34])	Ultimate strength (MPa)	30 (23 °C)
	Tensile adhesion strength (MPa)	Concrete fracture (> 4 N/mm <sup>2</sup> ) on sandblasted substrate
	Elastic modulus (GPa)	4.5 (23 °C)

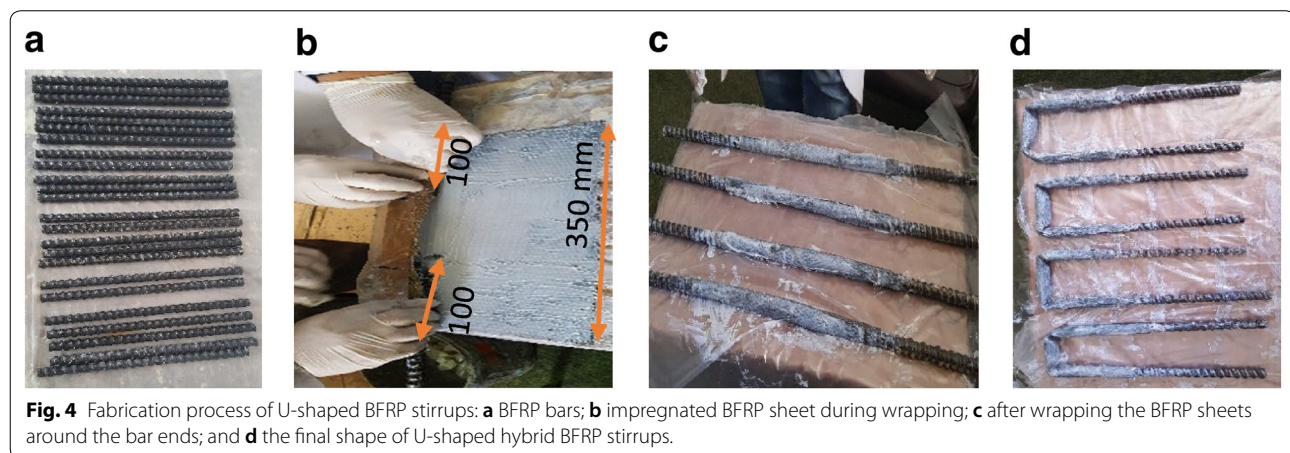


**Fig. 4** Fabrication process of U-shaped BFRP stirrups: **a** BFRP bars; **b** impregnated BFRP sheet during wrapping; **c** after wrapping the BFRP sheets around the bar ends; and **d** the final shape of U-shaped hybrid BFRP stirrups.

(Mofidi et al. 2012). For this anchorage method, BFRP bars were bonded to predrilled holes through the flange of the beam with epoxy. (2) The BFRP was anchored through the flange using ETS anchorage and through the web by using manually made U-shaped BFRP stirrups. (3) The BFRP was anchored through the web and flange by using manually made closed stirrups. The following sections provide the details for these anchors.

### 3.3.1 Manual Made U-shaped BFRP Stirrups

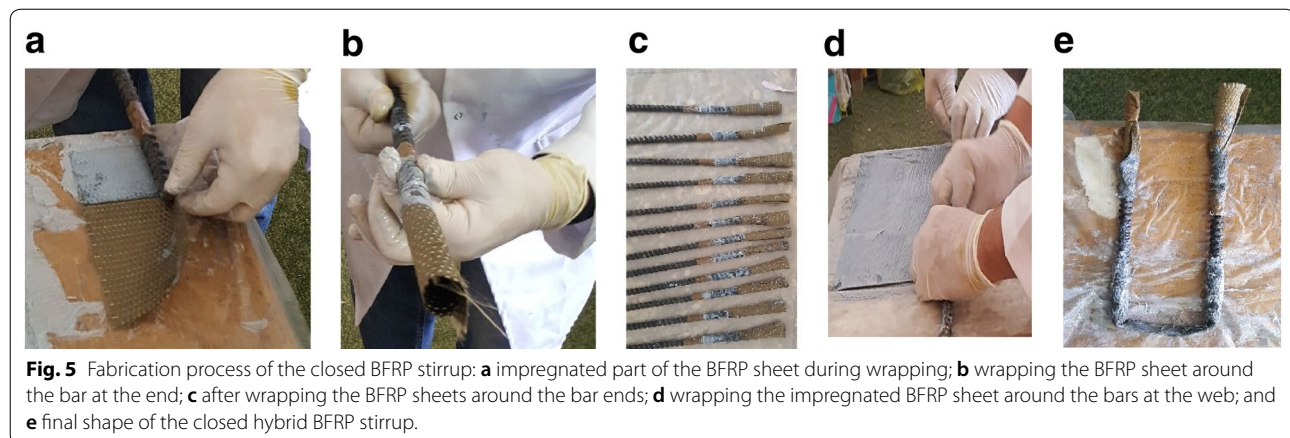
Figure 4 shows the manufacturing process of the U-shaped BFRP stirrups, which were adopted as the shear reinforcement for the beams. The reinforcement consisted of two BFRP bars (Fig. 4a) with diameters of 14 mm and lengths of 270 mm and BFRP sheets with dimensions of 200 × 350 mm. The BFRP sheet was impregnated with epoxy resin (Sikadur® 330) and wrapped around BFRP bars with an overlap length of 100 mm for each one, as shown in Fig. 4b, c. The direction of the fibers was in the longitudinal direction of the bars. After wrapping the BFRP sheets around the two bars, a straight shape was bent to form the U-shape, as shown in Fig. 4d.

### 3.3.2 Manually Manufactured Closed BFRP Stirrups

Figure 5 shows the manufacturing process of the closed BFRP stirrups, which is adopted as the shear reinforcement for the beams. They are made from a BFRP sheet wrapped around the BFRP bar ends where the fibers are in the direction of the bars. Both BFRP sheets have dimensions of 100 mm in width × 200 mm in length (fiber direction). The BFRP sheets are impregnated with epoxy resin and wrapped around the bar ends seventy millimeters from the length, as shown in Fig. 5a. The remaining parts of the BFRP sheets, 130 mm, are left dry and wrapped, as shown in Fig. 5b. After that, the other ends of the BFRP bars are connected with the BFRP sheets in a similar way as that of the U-shaped BFRP stirrups shown in Fig. 4. The bar is bent to have a U-shape with the unimpregnated BFRP sheets at the ends, as shown in Fig. 5d, which will be bonded together to form closed stirrups during installation after cutting them into a fan shape.

### 3.3.3 Strengthening Procedure and Instrumentation

The tested beams were strengthened in shear using the NSM techniques shown in Fig. 6. BFRP bars with a diameter of 14 mm were adopted, and two different



spacings “S” were considered, equal to 100 mm and 200 mm on both sides of the beams. The groove size was 25 mm wide and 22 mm deep, as shown in Fig. 6a. The grooves were made in the concrete cover of the RC beams using rectangular wooden sticks attached to the wooden formwork to locate grooves for the NSM-BFRP bars. After the concrete was cured, the wooden sticks were removed from the concrete specimens, and the surfaces of the grooves were grinded to increase the friction between the adhesive and concrete. The length of the groove was equal to the depth of the beam, which meant that the grooves continued with holes drilled through the flange of the beam. After the grooves were cleaned with acetone, they were half-filled with epoxy adhesive (Sikadur® 30) (Fig. 6b) followed by inserting the BFRP bars and U-shaped or closed BFRP stirrups, as shown in Fig. 6b, c. The bottom corners of the grooves were rounded off with epoxy adhesive to decrease stress concentration in the BFRP sheets. Finally, the grooves were filled with epoxy adhesive, and the surface was leveled as shown in Fig. 6d. In the case of strengthening

using BFRP closed stirrups, the T-beam was inverted, and the remaining dry fiber sheets were cut to strips similar to a fan shape and impregnated with epoxy, as shown in Fig. 7. The strips overlapped around the cross section to form closed stirrups. The specimens were cured at room temperature for 10 days.

The tested beam details are presented in Table 5 and the designation symbols are used hereafter. Beam TBC was tested as the control beam that had no strengthening. The notation for strengthened beam TBS100-ii is as follows: the three letters after ‘TBS’ refer to the spacing between the vertical BFRP bars (that is, S100: 100 mm or S200: 200 mm). The symbol after the dash refers to the type of NSM strengthening, which are “ii” for NSM strengthening with BFRP side bars (type 1 anchorage), “U” for NSM strengthening with manually made U-shaped BFRP stirrups (type 2 anchorage), and “[ ]” for NSM strengthening using manually made BFRP closed stirrups (type 3 anchorage).

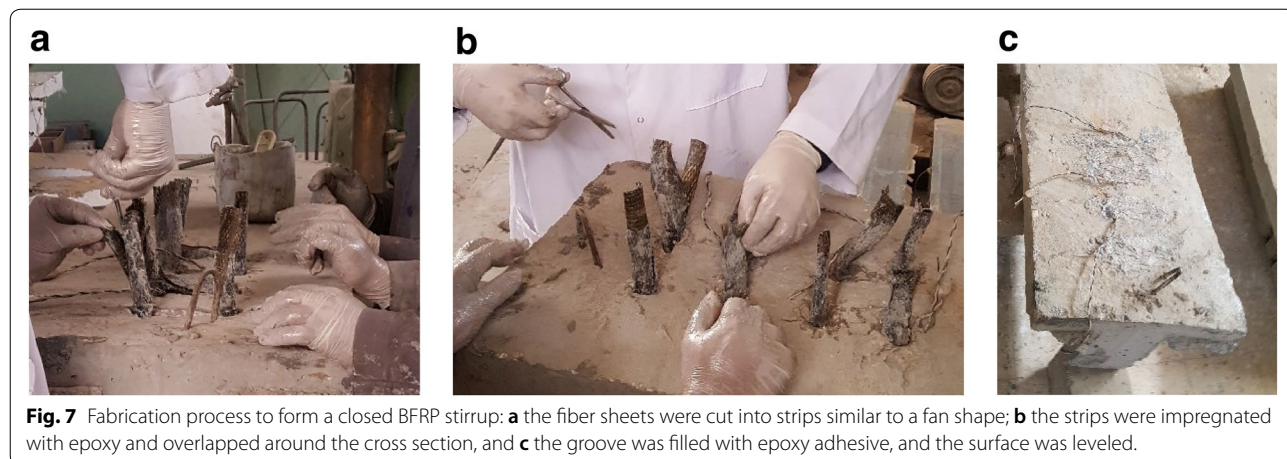


**Table 5** Properties of the concrete and specimen details.

Beam specimen	$F_{cu28}$ (MPa)	$F_{cu}$ (MPa) At test day	Type of strength.	Spacing "S" (mm)
TBC	25.1	27.8	–	
TBS200-ii	25.5	28.9	Bars	200
TBS200-[]	26.2	28.4	Closed stirrups	200
TBS100-ii	31	34	Bars	100
TBS100-U	27.1	32.7	U-stirrups	100
TBS100-[]	30.5	36.5	Closed stirrups	100

Each specimen was internally instrumented with four strain gauges attached at a critical position on the steel reinforcement prior to casting of the beams, as shown in Fig. 8. Two strain gauges (SSG-1 and SSG-2) were attached on the tension and compression longitudinal steel reinforcement, and the other two strain gauges (SSG-3 and SSG-4) were attached to steel stirrups at the weak shear side of the beams. Externally, each specimen was monitored using a linear variable displacement transducer (LVDT) placed under the applied load to measure the maximum deflection of the beam. In addition, other strain gauges (BFSG-n, where the number of strain gauges "n" depend on the number of BFRP bars) were installed on the BFRP bars 120 mm from the soffit of the beam, with one strain gauge for each BFRP bar. The crack initiation and the crack width at the weak shear side of the tested beams were monitored using a strain gauge attached on the web of the cross section and a crack width gauge attached perpendicularly at the critical position over the line between the support and point of loading. The three-point beam bending tests (Fig. 9) were carried out using a 600-kN hydraulic test machine, and the applied load was recorded with

a 2000-kN load cell. The loads and instruments were computerized and recorded data using an electronic data logger system at a sampling rate of 1 Hz. Crack propagation was marked during the test on the other side away from the instruments.

## 4 Experimental Results and Discussion

### 4.1 Overall Response

Table 6 summarizes the test results by listing the ultimate loads, the maximum shear capacities, the cracking loads, the deflection corresponding to the ultimate load, the failure modes of the tested beams, and the percentage of the shear capacity increase with respect to the control beam (TBC). The cracking load is obtained based on the developed strain of the concrete. It is worth noting that the cracking load of the NSM-BFRP-strengthened beams is close to that of the control beam and depends on the concrete strength. The use of NSM-BFRP bars is an effective technique for enhancing the shear capacity of RC beams, as shown in Table 6. The increase in the shear capacity of the strengthened beam ranges from 8.4 to 81.5% depending on both the spacing between the BFRP bars and the type of anchor. The shear capacity of beams TBS200-ii and TBS200-[] increased by 8.3% and 39.6%, respectively. However, the shear capacity increased by 46.3%, 81.5%, and 50.7% for beams TBS100-ii, TBS100-U, and TBS100-[], respectively. These improvements in the shear capacity of the strengthened beams emphasized the effectiveness of both the U-shaped BFRP stirrups and BFRP closed stirrups. The improvement in the shear capacity of beam TBS100-U is higher than that of beam TBS100-[]. This is attributed to the fact that the failure of beam TBS100-[] occurred due to concrete crushing at the support zone. Hence, the performance of U-shaped stirrups were found to be at least similar to that of BFRP closed stirrups, and the ETS anchorage

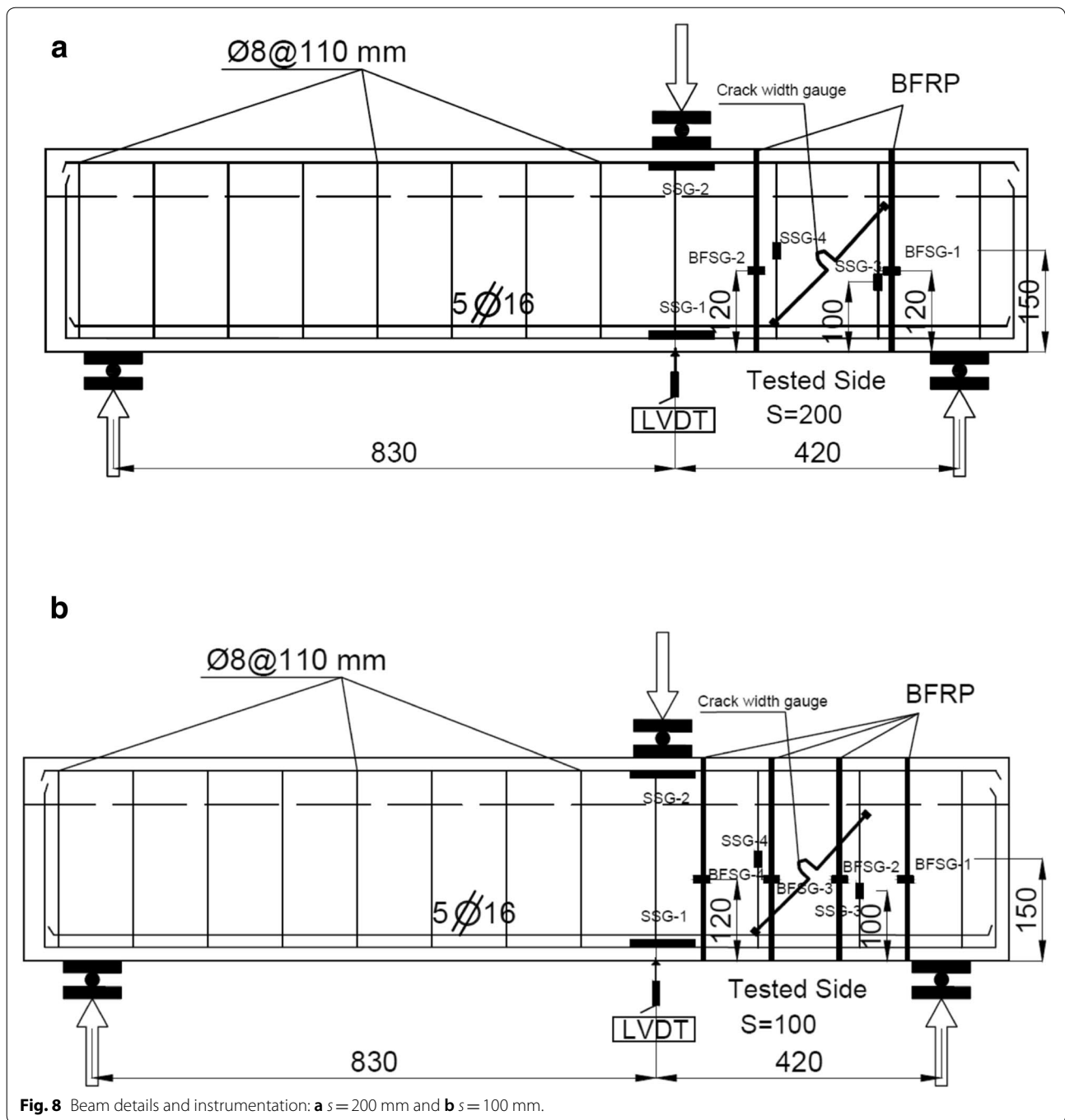


**Fig. 8** Beam details and instrumentation: **a**  $s = 200$  mm and **b**  $s = 100$  mm.

through the flange was sufficient and there was no need for closed stirrups for T-cross section beams. The effectiveness of closed BFRP stirrups was expected to be clear for rectangular sections, which was out of the scope of this study and needs to be studied. Due to the presence of the proposed anchorage, the shear capacity increased by 24% to 29% compared to that of the corresponding beams without anchorage. The gained shear force for specimens

TBS100-[] was excluded because failure was due to crushing of the concrete at the support zone.

#### 4.2 Influence of the Spacing Between the BFRP-NSM Bars

The shear capacity improvement was dependent on the spacing “S” between the BFRP bars where TBS200-ii and TBS100-ii increased by 8.3% and 46.3%, respectively, and the shear capacity of beams TBS200-[] and TBS100-[]

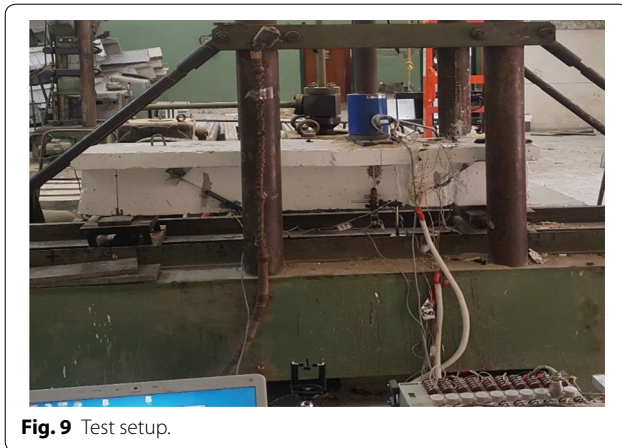


**Fig. 9** Test setup.

increased by 39.6% and 50.7%, respectively, based on the control specimen. Consequently, the shear capacity increased by 30% to 35% due to reduced spacing between the BFRP bars compared to the corresponding beams. Similar behavior was observed by Rizzo and De Lorenzis (2009); however, this behavior was contradicted by Wiwatrojanagul et al. (2012), who noticed that decreasing the spacing between the NSM-FRP bars resulted in concrete cover splitting failure. The presence of the proposed anchorage prevented premature debonding.

#### 4.3 Load–Deflection Curve

The load–deflection curves of the different tested beams are shown in Fig. 10. The recorded deflection represents the deflection at the point of the load application. Prior to reaching the ultimate load, the behavior among all the beams is almost similar, indicating that the flexural stiffness of the beams is not substantially affected by the application of NSM-BFRP shear strengthening. However, the strengthening technique results in considerable increases in the ultimate loads, and in turn, the shear capacity of the beams increase. Moreover, strengthening of the beams increases their ductility, where the deflection corresponding to the ultimate loads increases by 30.6% to 181.9% depending on both the spacing between the NSM bars and the type of anchorage, as shown in Table 6.

By comparing the results for the strengthened beams, it is clear that both the U-shaped and closed BFRP stirrups contributed to the increased effectiveness in the shear strengthening with BFRP bars compared to that of the control specimen. Anchoring around the web at the soffit of the beams prevented sudden debonding of the first NSM-BFRP bar from the support, as will be discussed later. An interesting observation from Fig. 10

is that no brittle failure was observed after reaching the ultimate loads even for the control beam (TBC) due to the contribution provided by the strong dowel action of the longitudinal reinforcement. However, the degradation of the load after reaching the ultimate load depended on the type of strengthening; specimens TBS200-ii and TBS100-ii had a higher degradation compared to that of specimens TBS200-[], TBS100-[], and TBS100-U. Such behavior could be observed because of the presence of anchorage around the web at the soffit of the beams, which prevented abrupt shear failure. The failure of specimen TBS100-U changed from shear failure to flexural failure, as shown in Fig. 10. Moreover, Fig. 11 shows the relationship between the load and longitudinal steel strain for a given load for different beams, which confirms the flexural failure of beam TBS100-U.

#### 4.4 Crack Pattern and Failure Modes

The cracking load level of the tested beams is shown in Table 6. The cracking load depends on the concrete strength rather than the strengthening type. The shear failure and crack pattern of different tested beams are shown in Fig. 12. During the loading of control beam TBC, a diagonal shear crack initiated at the middle of the shear span at approximately mid-height of the beam at a load of 80 kN. This crack propagated toward the support and point of loading as the load increased, forming a major diagonal shear crack at an angle of 48° (Fig. 12a), and it widened until failure at a load of 227 kN (shear failure, SF). Specimen TBS200-ii, the beam strengthened with NSM-BFRP bars without anchoring at the soffit of the beam, experienced the first diagonal shear crack at a load of 72 kN at an angle of 45°. As the load increased, the first shear crack propagated and crossed the first BFRP bar, and then another shear crack formed just after the end of the first BFRP bar from the support at an angle of 60°. A popping noise was noted throughout the test, revealing the sudden debonding of the first BFRP bar from the support and the failure of the beam, as shown in Fig. 12b. Beam TBS200-ii failed at a load level of 246 kN due to the debonding between the BFRP bar and the epoxy (DE) at the end of the BFRP bars. This failure mode occurred due to the large spacing between the NSM bars. This failure mode was also observed by other researchers (De Lorenzis and Nanni 2001; Bianco et al. 2009; Rahal and Rumaih 2011).

Typical shear cracks developed in TBS100-ii, where the first shear crack appeared at a load level of 110 kN and failure occurred at a load level of 332 kN. The number of cracks was greater than the number of cracks noticed in TBS200-ii; the cracks crossed the BFRP bars,

**Table 6 Test results.**

Beam Specimen	Cracking		Ultimate Load ( $P_u$ ) kN	Ultimate Shear kN	Deflection At $P_u$ (mm)	Increase over reference beam (%)		Increase in shear force (%) due to			Failure Mode <sup>a</sup>
	Load kN	Load kN				Ultimate load	Deflection (at $P_u$ )	Anchorage kN	Spacing	Max. BFRP Strain ( $\mu\epsilon$ )	
TBC	80	227	150.7	3.37	-	-	-	-	-	-	SF
TBS200-II	72	246	163.3	4.4	8.3	30.6	-	-	-	4470	DE
TBS200-I	77	317	210.5	5.9	39.6	75.1	29	-	-	4519	SF
TBS100-II	110	332	220.5	5.08	46.3	50.74	-	35	-	3450	CCS
TBS100-U	90	412	273.6	9.5	82	181.9	24	30	-	7612	FF
TBS100-I	94	342	227.1	6.01	50.7	78.3	3	8	-	6308	SF&CCZ

<sup>a</sup> SF, DE, CCS, CCZ, and FF correspond to shear failure, debonding epoxy, concrete cover splitting, crushing of the concrete at the support zone, and flexural failure.

and failure occurred due to the debonding of the second BFRP bar in the location with a relatively small anchorage length at the soffit of the beam. The lower part of the second BFRP bar from the support along with the epoxy and part of the surrounding concrete split away from the main concrete of the beam, as shown in Fig. 12c. This type of debonding is referred to as concrete cover splitting (CCS) and is due to an insufficient anchorage length, which is similar to the failure mode observed by Rahal and Rumaih (2011).

For specimens with anchors around the web of the beam (i.e., TBS200-[], TBS100-[], and TBS100-U), diagonal shear cracks started to open up at a relatively equal spacing, and the angles of cracks to the beam axis were  $40^\circ$  to  $63^\circ$ . These cracks initiated approximately at the soffit of the beam and propagated diagonally crossing the vertical BFRP bars. The cracks did not appear under the epoxy-filled grooves as the modulus of elasticity of the epoxy is lower than that of the concrete and the epoxy has a higher ductility. With increasing load, the evaluation of the cracking pattern differed between the beams with various spacings between the NSM-BFRP bars. For specimen TBS200-[], the first shear crack initiated at a load of 77 kN, and the failure load was 317 kN. Three of the cracks that crossed the BFRP bars widened considerably before failure within the space between the BFRP bars; see Fig. 12d. For specimen TBS100-[], the cracked load and failure load were 94 kN and 342 kN, respectively. The failure of TBS100-[] was due to the enlargement of the diagonal shear cracks (shear failure) at the shear zone, and sudden failure occurred due to crushing of the concrete at the support zone (CCZ); see Fig. 12e. This type of failure was likely due to an insufficient quantity of stirrups in this zone due to poor detailing by the authors during the planning stage. It should be mentioned that adding additional stirrups beyond the support might have prevented this failure mode from occurring. Consequently, it could be concluded that the failure of specimen TBS100-[] was not only due to shear. Both the cracking and failure loads of specimen TBS100-U were 90 kN and 410 kN, respectively. After the initiation of the diagonal shear cracks that crossed the BFRP bars, one dominant crack initiated with an angle of  $69^\circ$  at the soffit of the beam, widened and propagated diagonally near the maximum bending moment zone. This crack occurred between the two BFRP bars near the point of loading, as shown in Fig. 12f. It is worth mentioning that strengthening the T-beam with U-shaped BFRP stirrups changed the failure mode of the beam from shear failure to flexure failure (Fig. 11). It is worth noting that the different beams strengthened with NSM-BFRP bars with anchorage failed due to the enlargement of the diagonal

cracks (shear failure) and had no debonding or concrete cover splitting at the strengthened zone even for small spacing values ( $S=100$  mm). This behavior contradicted that obtained by Wiwatrojanagul et al. (2012). Providing the additional anchorage of the NSM-BFRP bars around the web of the beam prevented the premature debonding of the NSM-BFRP bars and in turn increased the effectiveness of the NSM-BFRP bars for enhancing the shear capacity of the beams.

#### 4.5 Load and Steel Stirrup Strain Relationship

Figure 13 shows the load versus steel strain curves obtained from the strain gauge attached to the second stirrup from the support of the beam at the tested shear span ("SSG4" shown previously in Fig. 8). It is worth noting that the steel strain is almost negligible up to cracking. Based on this phenomenon, the cracking loads of different tested beams were recorded as previously reported in Table 6. Once the first crack of the tested beam is formed, the strain induced in the steel stirrups increases considerably with increasing applied load, and the relationship depends on the type of strengthening. The relationship between the load and the measured strain shown in Fig. 13 gives essential information for quantifying the effect of the strengthening type. The strain in the steel stirrups of beam TBC increases at a faster rate with increasing load, and the stirrups yielded at a much lower load compared to those of the strengthened beams. Moreover, the strain in the steel stirrups of beams TBS200-[], TBS100-[], and TBS100-U increased at a lower rate than the control beam, and the stirrups yielded until reaching their failure loads, which was also observed by Anwarul (2009). However, the beams strengthened in shear without anchorage (TBS200-ii and TBS100-ii) failed in shear prior to the yielding of the stirrups, which was also observed by Chen et al. (2013). Consequently, the yield stress of the steel stirrups in such strengthened beams cannot be fully utilized. It is worth noting that the efficiency of the anchorage between the BFRP bars and sheets with lengths equal to 100 mm (Fig. 4b) for U-shaped and closed stirrups has been verified because no debonding or slipping occurred at these connections.

#### 4.6 Load–BFRP Strain Relationship

The load versus the maximum measured BFRP strains at the critical shear location are shown in Fig. 14. The maximum strain is measured in the NSM bars that intercepted the major shear crack of the RC beams. It is worth noting that the BFRP strains are almost negligible up to cracking, which has a similar tendency to

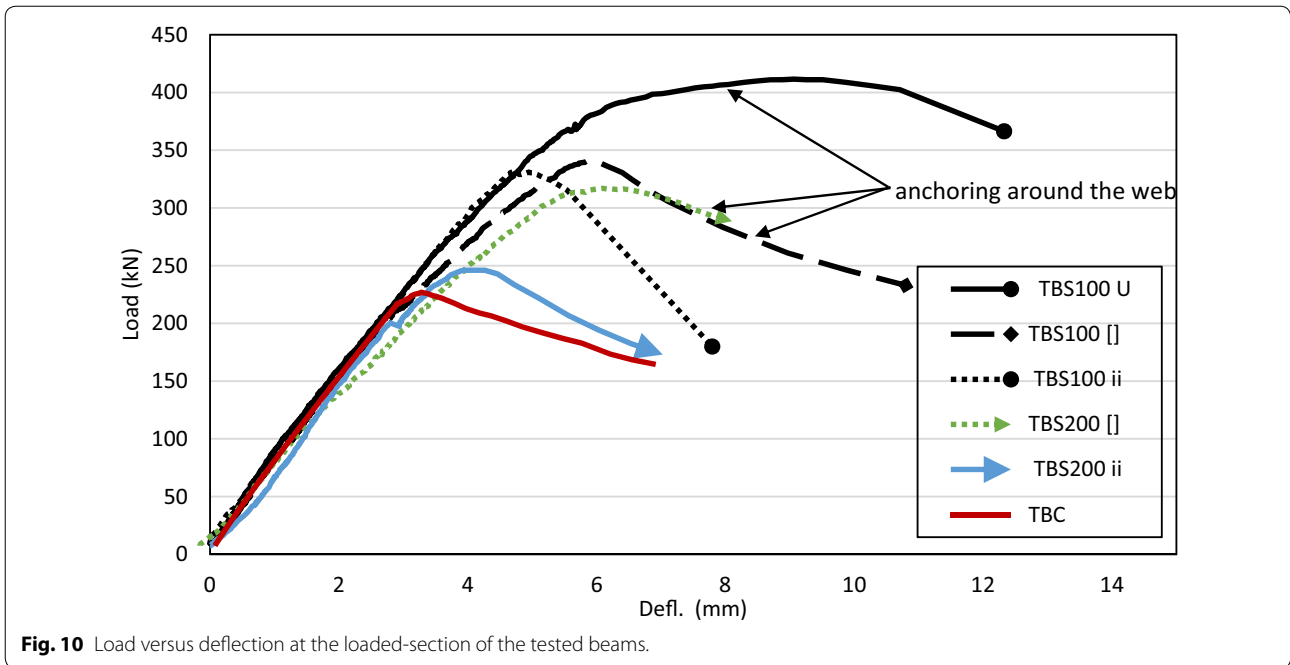


**Fig. 10** Load versus deflection at the loaded-section of the tested beams.

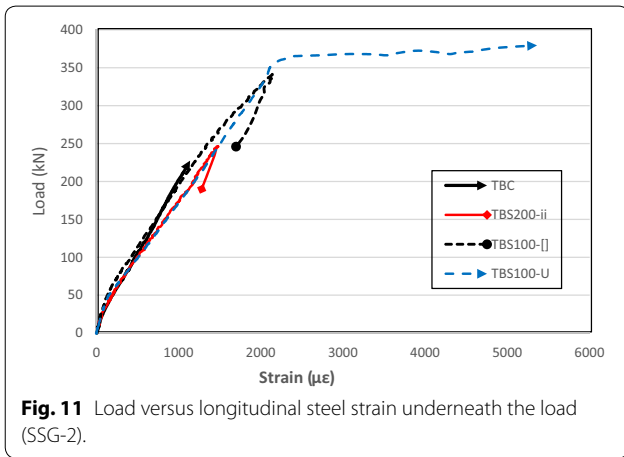


**Fig. 11** Load versus longitudinal steel strain underneath the load (SSG-2).

those of the steel stirrups shown previously in Fig. 13. In the next part of the curve, the strain in BFRP bars increases up to the ultimate load for all the strengthened beams due to the transfer of the force to the BFRP bars after cracking. However, beyond the ultimate load, the load versus strain relationship behavior depends on the type of anchorage. The strains of beams TBS200-ii and TBS100-ii start to decrease drastically after reaching the ultimate loads. This implies that sudden debonding occurred, which results in the interaction between the concrete, steel stirrups and BFRP side bars being ignored. This behavior is also

reported by Mofidi et al. (2016), where the beams are strengthened without anchoring. However, specimens TBS200-[], TBS100-[], and TBS100-U, which are strengthened using closed or U-shaped BFRP stirrups, show softening behavior beyond the ultimate load. The increasing strain of the BFRP bars with the reduction in the load is due to the presence of the interaction between the concrete, steel stirrups, and BFRP stirrups. The effective strain of the BFRP bars depends on the type of anchoring and reaches 27–35% of its maximum strain for beams TBS200-ii and TBS100-ii. This ratio of the effective strain to the ultimate strain is very similar to that observed by Anwarul (Anwarul 2009) (30–35%), where NSM CFRP is used to strengthen concrete beams without anchoring. However, the effective strain of the BFRP bars is within a range of 35–59% of its ultimate strain for beams TBS200-[], TBS100-[], and TBS100-U.

#### 4.7 Shear Crack Width

For all the different beams, the crack width of the concrete along the shear span was determined using a clip gauge with a length of 250 mm attached at the mid-height of the cross section and perpendicular to the line between the support and the point of loading for all tested beams. It is worth mentioning that all the cracks for the tested beams occurred through the crack width device. Figure 15 shows the total width of the shear cracks for all the



**Fig. 12** Failure modes and crack patterns of the tested beams.

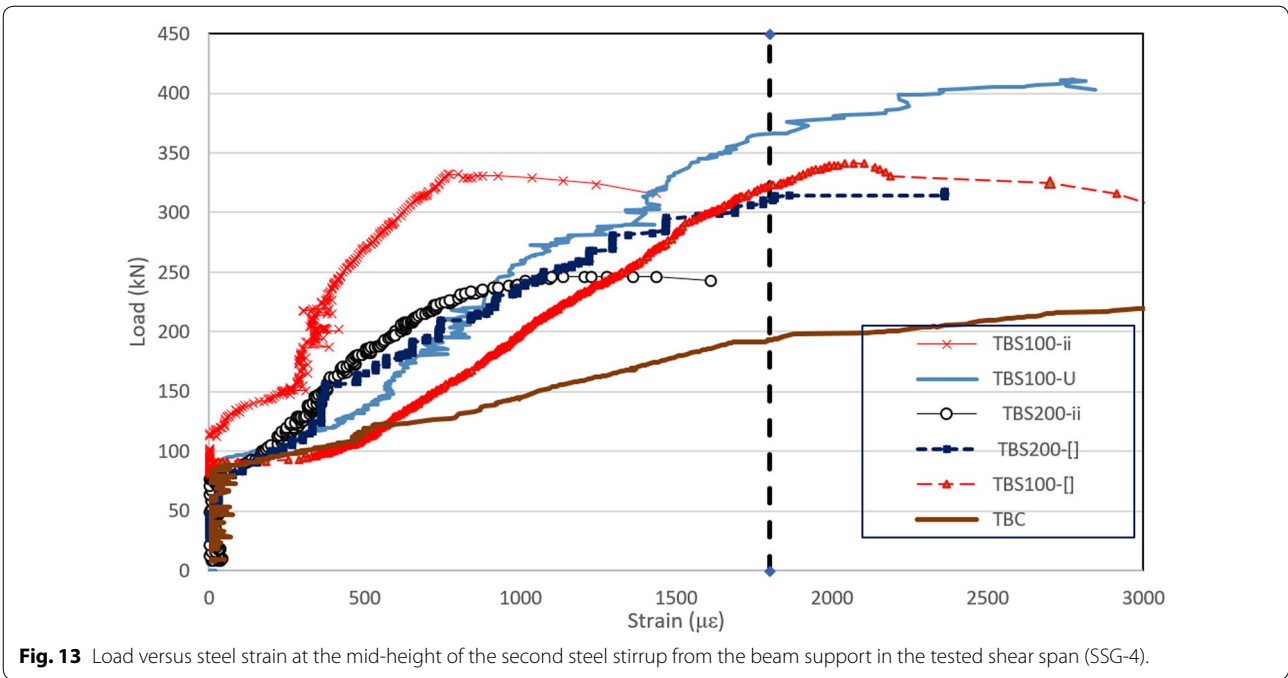


**Fig. 13** Load versus steel strain at the mid-height of the second steel stirrup from the beam support in the tested shear span (SSG-4).

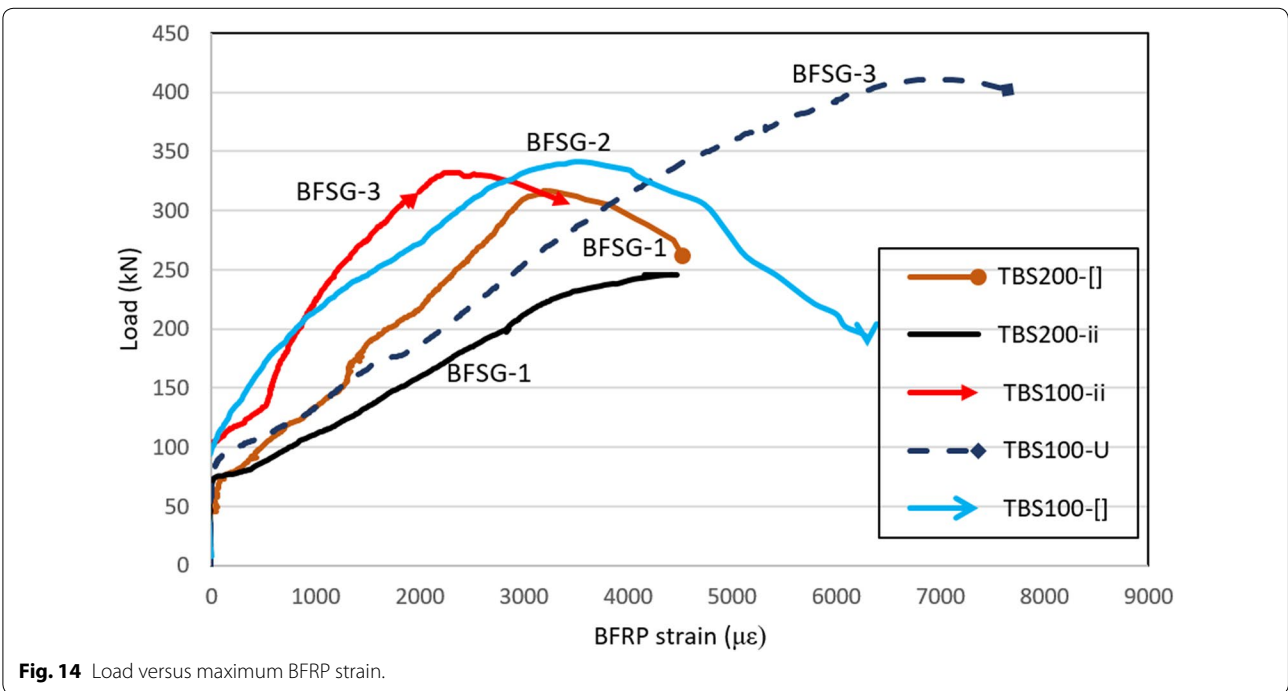
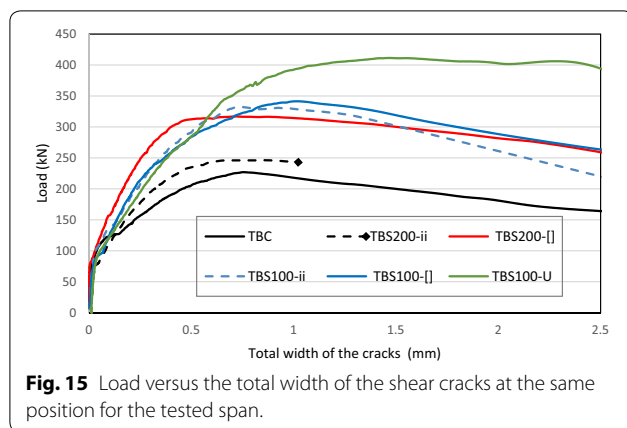


**Fig. 14** Load versus maximum BFRP strain.

tested beams. Strengthening the beams with NSM-BFRP bars resulted in a reduction in the crack width at the same load level compared with that of the control beam (TBC). This improvement in the crack width depended

on the spacing between the NSM-BFRP bars and the type of anchor. Specimen TBS200-ii exhibited a relatively limited improvement in the crack width and ductility due to sudden debonding of the first NSM-BFRP bar from the



support. The ultimate load occurred at a crack width equal to 0.75 mm for the control beam (TBC), while the ultimate loads for the strengthened beams occurred at different values ranging from 0.47 to 1.02 mm.

## 5 Conclusions

This study reported an experimental program that investigated the behavior of RC T-beams strengthened in shear with NSM-BFRP bars. The contribution of the BFRP bars in shear strengthening was experimentally assessed with six T-section RC beams. Moreover, a manual nonmechanical anchorage was developed, and its effectiveness was evaluated. The main findings of this study were stated as follows:

- The test results showed that the NSM method using BFRP bars enhanced the shear capacity of RC T-beams, and the BFRP bars could be used as a shear-strengthening material for RC beams.
- The test results emphasized that the use of the proposed anchorage enhanced the shear capacity of RC beams. The increase in the shear capacity, based on the reference beam, ranged between 8.3 and 46% for beams strengthened with NSM-BFRP bars without anchorage, and the increase ranged between 39.6 and 81.6% for beams strengthened with NSM-BFRP bars with the proposed anchor.
- The test results assured that the use of the proposed anchorage enhances the shear contribution of the NSM bars. The maximum strains of the BFRP bars ranged from 27 to 35% from their ultimate strain for strengthened beams without anchorage. However, these values ranged from 35 to 59% for beams strengthened with the proposed anchorage.
- Beams strengthened without anchorage failed due to the debonding of the NSM-BFRP bars before the internal steel stirrups yielded in contrast to the

beams strengthened with NSM-BFRP bars using the proposed anchorage. Thus, internal steel stirrups may have contributed less than what was predicted by existing shear strength models.

- The test results showed that ETS end anchorage for U-shaped BFRP stirrups through the flange of the RC T-beams was sufficient and there was no need for the closed BFRP stirrup technique.

### Authors' contribution

HMD; Designed and performed experiments, analysed data, analyzed the experimental results, and wrote the original draft preparation. AMS; co-wrote the paper and co-analyzed the experimental results. All authors read and approved the final manuscript.

### Authors' information

Hesham M. Diab, Associate Prof., Civil Engineering Department, Faculty of Engineering, Assiut University, Assiut, Egypt  
 Ahmed M. Sayed, Assistant Prof., Civil Engineering Department, Faculty of Engineering, Assiut University, Assiut, Egypt (on leave to Civil and Environmental Engineering Department, Majmaah University, Majmaah, KSA)

### Competing interests

The authors declare that they have no competing interests.

### Author details

<sup>1</sup> Civil Engineering Department, Faculty of Engineering, Assiut University, Assiut, Egypt. <sup>2</sup> Department of Civil and Environmental Engineering, College of Engineering, Majmaah University, Al-Majmaah, Kingdom of Saudi Arabia.

Received: 25 February 2020 Accepted: 13 July 2020

Published online: 09 September 2020

### References

- American Concrete Institute (2004). Guide test methods for fiber-reinforced polymers (FRPs) for reinforcing or strengthening concrete structures. ACI 440.3R-04, Farmington Hills, MI.
- American Concrete Institute (2015). Guide for the design and construction of structural concrete reinforced with Fiber-Reinforced Polymer (FRP) bars. ACI 440.1R-15, Farmington Hills, MI.
- American Society for Testing and Materials (ASTM) (1997). Standard Test Methods and Definitions for Mechanical Testing of Steel Products. ASTM A370-97a, West Conshohocken, PA.
- Anwarul, A. K. M. (2009). Effective methods of using CFRP bars in shear strengthening of concrete girders. *Engineering Structures*, 31(3), 709–714.
- Barros, J. A. O., & Dias, S. J. E. (2006). Near surface mounted CFRP laminates for shear strengthening of concrete beams. *Cement and Concrete Composites*, 28(3), 276–292.
- Bianco, V., Barros, J. A. O., & Monti, G. (2009). Three dimensional mechanical model for simulating the NSM FRP strips shear strength contribution to RC beams. *Engineering Structures*, 31(4), 815–826.
- Bilotta, A., Ceroni, F., Nigro, E., & Pecce, M. (2015). Efficiency of CFRP NSM strips and EBR plates for flexural strengthening of RC beams and loading pattern influence. *Composite Structures*, 124, 163–175.
- Chen, W., Pham, T., Sichebe, H., Chen, L., & Hao, H. (2018). Experimental study of flexural behaviour of RC beams strengthened by longitudinal and U-shaped basalt FRP sheet. *Composite Part B*, 134, 114–126.
- Chen, G. M., Teng, J. G., & Chen, J. F. (2013). Shear strength model for FRP-strengthened RC beams with adverse FRP-steel interaction. *Journal of Composites for Construction*, 17(1), 50–66.
- De Lorenzis, L., & Nanni, A. (2001). Shear strengthening of reinforced concrete beams with NSM fiber-reinforced polymer rods. *Structural Journal*, 98(1), 60–68.
- Diab HM, Wu Z (2009). Bond Behaviour of Different FRP Sheets. In: Proceedings of the 9<sup>th</sup> International Symposium of the Fiber-Reinforced Polymer

- Reinforcement for Reinforced Concrete Structures (FRPRCS-9), Sydney, Australia.
- Diab, H. M., Wu, Z., & Iwashita, K. (2009). Short and long-term bond performance of prestressed FRP sheet anchorages. *Engineering Structures*, 31(5), 1241–1249.
- Dias, S. J. E., & Barros, J. A. O. (2010). Performance of reinforced concrete T beams strengthened in shear with NSM CFRP laminates. *Engineering Structures*, 32(2), 373–384.
- Dias, S. J. E., & Barros, J. A. O. (2011). Shear strengthening of RC T-section beams with low strength concrete using NSM CFRP laminates. *Cement and Concrete Composites*, 33(2), 334–345.
- Egyptian Code of Practice (2007). Design and Construction for Reinforced Concrete Structures. ECP 203-2007, Research Center for Housing, Building and Physical Planning, Cairo, Egypt.
- Elmahdy, A., & Verleysen, P. (2020). Mechanical behavior of basalt and glass textile composites at high strain rates: A comparison. *Polymer Testing*, 81, 106224.
- Jalali, M., Sharbatdar, M. K., Jian-Fei, Chen, & Alaei, F. J. (2012). Shear strengthening of RC beams using innovative manually made NSM FRP bars. *Construction and Building Materials*, 36, 990–1000.
- Kalfat, R., Al-Mahaidi, R., & Smith, S. T. (2013). Anchorage devices used to improve the performance of reinforced concrete beams retrofitted with FRP composites: State-of-the art review. *Journal of Composites for Construction*, 17(1), 14–33.
- Kemapoxy 165. Non-Shrink Epoxy adhesive Mortar and Grouting Compound and for fixing steel bars into concrete under water. [http://cmbegypt.com/cmb/en/wp-content/pdf/Chemical\\_construction/06\\_construction\\_repair\\_strengthening/5.kemapoxy%20165/kemapoxy%20165.pdf](http://cmbegypt.com/cmb/en/wp-content/pdf/Chemical_construction/06_construction_repair_strengthening/5.kemapoxy%20165/kemapoxy%20165.pdf)
- Koutas, L., & Triantafillou, T. C. (2013). Use of anchors in shear strengthening of reinforced concrete T-beams with FRP. *Journal of Composites for Construction*, 17(1), 101–107.
- Lebedev, M. P., Startsev, O. V., & Kychkin, A. K. (2020). The effects of aggressive environments on the mechanical properties of basalt plastics. *Heliyon*, 6(3), e03481.
- Mofidi, A., Chaallal, O., Benmokrane, B., & Neale, K. W. (2012). Experimental tests and design model for RC beams strengthened in shear using the embedded through-section FRP method. *Journal of Composites for Construction*, 16(5), 540–550.
- Mofidi, A., Chaallal, O., Cheng, L., & Shao, Y. (2016). Investigation of near surface-mounted method for shear rehabilitation of reinforced concrete beams using fiber reinforced-polymer composites. *Journal of Composites for Construction*, 20(2), 1–14.
- Rahal, K. N., & Rumaih, H. A. (2011). Tests on reinforced concrete beams strengthened in shear using near surface mounted CFRP and steel bars. *Engineering Structures*, 33(1), 53–62.
- Rizzo, A., & De Lorenzis, L. (2009). Behavior and capacity of RC beams strengthened in shear with NSM FRP reinforcement. *Construction and Building Materials*, 23, 1555–1567.
- Sharbatdar, M. K., & Jaber, M. (2018). Flexural and shear strengthening of RC beams with NSM technique and manually made CFRP bars. *Scientia Iranica*, 25(4), 2012–2025.
- Shekarchi, A., Ghannoum, W. M., & James, J. W. (2018). Use of anchored carbon fiber-reinforced polymer strips for shear strengthening of large girders. *ACI Structural Journal*, 115(1), 281–291.
- Sikadur®-330. Product Data sheet-adhesive for bonding reinforcement. [https://egy.sika.com/dms/getdocument.get/b5ed2585-b802-3ef0-8825-c669a8542e3/Sikadur\\_330.pdf](https://egy.sika.com/dms/getdocument.get/b5ed2585-b802-3ef0-8825-c669a8542e3/Sikadur_330.pdf)
- Sim, J., Park, C., & Moon, D. Y. (2005). Characteristics of basalt fiber as a strengthening material for concrete structures. *Composites Part B: Engineering*, 36, 504–512.
- Sundarraja, M. C., & Rajamohan, S. (2009). Strengthening of RC beams in shear using GFRP inclined strips—an experimental study. *Construction and Building Materials*, 23, 856–864.
- Shanxi Basalt Fiber Technology Co., Ltd [http://www.sxcbf.com/en/sjxmore.asp?c\\_id=48&hidden=39](http://www.sxcbf.com/en/sjxmore.asp?c_id=48&hidden=39)
- Sikadur®-30. Product Data sheet-adhesive for bonding reinforcement. <https://egy.sika.com/dms/getdocument.get/a470020f-8c78-314e-89f1-3862b856077f/Sikadur%20-30.pdf>
- Wang, X., Shi, J., Liu, J., Yang, L., & Wu, Z. (2014). Creep behavior of basalt fiber reinforced polymer tendons for prestressing application. *Materials and Design*, 59, 558–564.
- Wang, Z., Zhao, X. L., Xian, G., Wu, G., Raman, R. S., Al-Saadi, S., et al. (2017). Long-term durability of basalt- and glass-fibre reinforced polymer (BFRP/GFRP) bars in seawater and sea sand concrete environment. *Construction and Building Materials*, 139, 467–489.
- Wiwatrojanagul, P., Ayudhya, B. I. N., & Sahamitmongkol, R. (2012). NSM FRP shear strengthening of RC beams with internal stirrups. *Thammasat International Journal Science Technology*, 17(1), 16–30.
- Wu, Z. S., Wang, X., Iwashita, K., Sasaki, T., & Hamaguchi, Y. (2010). Tensile fatigue behaviour of FRP and hybrid FRP sheets. *Composites Part B Engineering*, 41, 396–402.

## Publisher's Note

Springer Nature remains neutral with regard to jurisdictional claims in published maps and institutional affiliations.

Submit your manuscript to a SpringerOpen® journal and benefit from:

- Convenient online submission
- Rigorous peer review
- Open access: articles freely available online
- High visibility within the field
- Retaining the copyright to your article

Submit your next manuscript at ► [springeropen.com](https://www.springeropen.com)